# Hybrid density functional calculations of the band gap of $Ga_xIn_{1-x}N$

Xifan Wu,[1] Eric J. Walter,[2] Andrew M. Rappe,[3] Roberto Car,[1] and Annabella Selloni[1]
[1]*Chemistry Department, Princeton University, Princeton, New Jersey 08544-0001, USA*
[2]*Department of Physics, College of William and Mary, Williamsburg, Virginia 23187-8795, USA*
[3]*The Makineni Theoretical Laboratories, Department of Chemistry, University of Pennsylvania, Philadelphia, Pennsylvania 19104-6323, USA*
(Received 11 July 2009; published 2 September 2009)

Recent theoretical work has provided evidence that hybrid functionals, which include a fraction of exact (Hartree-Fock) exchange in the density functional theory exchange and correlation terms, significantly improve the description of band gaps of semiconductors compared with local and semilocal approximations. Based on a recently developed order-*N* method for calculating the exact exchange in extended insulating systems, we have implemented an efficient scheme to determine the hybrid functional band gap. We use this scheme to study the band gap and other electronic properties of the ternary compound $In_{1-x}Ga_xN$ using a 64-atom supercell model.

DOI: 10.1103/PhysRevB.80.115201 PACS number(s): 71.15.Dx, 71.15.Mb, 71.20.Nr

## I. INTRODUCTION

The design of novel functional semiconductors with given values of the energy band gap is an area of intense research.[1–6] In particular, much attention is focused on the band-gap engineering of group-III nitride semiconductors, whose remarkable optical properties are important for optoelectronic device applications.[7,8] To guide the search for compounds with tailored properties,[1] experimental studies are often accompanied by electronic-structure calculations based on density functional theory (DFT).[9] For these calculations, the local-density approximation (LDA) or generalized gradient approximation (GGA) are typically used. Due to the delocalization error of the LDA and GGA exchange and correlation functionals, however, these approaches severely underestimate the materials band gaps.[10,11]

As shown by several recent studies,[12] a significant improvement in the description of semiconductor and insulator band gaps is generally obtained by using hybrid functionals,[13] in which some exact (Hartree-Fock) exchange is mixed into the exchange and correlation functional. This reduces the delocalization and derivative discontinuity errors of (semi)local functionals.[2,10–12] However, because of the considerable computational cost of evaluating the nonlocal exact exchange term, hybrid functionals have been mostly applied to systems with small unit cells.[14] For the modeling of systems where a large supercell is needed, an additional screened exchange approximation is usually made to relieve the computational burden.[2,12]

Recently Wu–Selloni–Car[15] (WSC) introduced an order-*N* method to calculate the exact exchange in extended insulating systems. The WSC method is based on a localized Wannier function representation of the occupied (valence) space, so that the exchange interaction between two orbitals decays rapidly with the distance between their centers. A truncation can thus be introduced, which greatly reduces the computational cost. The effectiveness of the WSC method was demonstrated by ground-state electronic minimizations for crystalline silicon in supercells with 64 and 216 atoms.

In this paper, we extend the WSC scheme to compute hybrid functional band gaps. To this end, the system's first (few) empty conduction state(s) is (are) determined starting from the ground state calculated via the WSC method. With hybrid functionals, this requires the computation of the pair exchange between the empty state and each valence orbital. Even though the empty state is delocalized, the product between this state and a valence orbital is well localized, so that the corresponding exchange interaction can be truncated as in the original WSC method.[15,16] We apply our scheme to determine the band gap of $In_{1-x}Ga_xN$, a ternary nitride semiconductor of great technological interest, and of its parent compounds, InN and GaN, using the PBE0 hybrid functional.[17] Our results show that, compared to the semilocal PBE functional, PBE0 gives a considerably improved description of the band gap, as well as of the cation *d*-state binding energy, which is also poorly described by the semilocal functionals.

## II. FORMALISM AND METHOD OF CALCULATION

The nonempirical PBE0 hybrid functional is constructed by mixing 25% of exact exchange with the GGA-PBE exchange[17] while the correlation potential is still represented by the corresponding functional in PBE,[18]

$$E_{xc}^{\mathrm{PBE0}} = \frac{1}{4}E_x + \frac{3}{4}E_x^{\mathrm{PBE}} + E_c^{\mathrm{PBE}}. \quad (1)$$

Here $E_x$ denotes the exact exchange energy, $E_x^{\mathrm{PBE}}$ is the PBE exchange, and $E_c^{\mathrm{PBE}}$ is the PBE correlation functional. $E_x$ has the usual Hartree-Fock form in terms of one-electron orbitals. In the WSC method, this term is expressed in terms of localized Wannier orbitals $\{\tilde{\varphi}_i\}$. These are obtained through an unitary transformation of the delocalized Bloch states $\{\varphi_i\}$ corresponding to occupied bands. In particular, we use maximally localized Wannier functions (MLWFs),[16] which are exponentially localized. In this way, a significant truncation in both number and size of exchange pairs can be achieved in real space.

We now turn to the calculation of the band gap. In extended insulating systems the band gap is simply given by

 

the difference between the eigenvalue of the highest occupied and the lowest empty state. Once the ground state has been minimized self-consistently, the eigenvalue of the empty state $\varphi_e$ can be obtained through a simple nonself-consistent calculation. With the hybrid PBE0 functional, the equation for $\varphi_e$ is

$$\left\{-\frac{1}{2}\nabla^2 + V_{\text{ion}}(\mathbf{r}) + V_{\text{H}}[\rho^{\text{val}}(\mathbf{r})] + \frac{3}{4}V_x^{\text{PBE}}[\rho^{\text{val}}(\mathbf{r})] + V_c^{\text{PBE}}[\rho^{\text{val}}(\mathbf{r})]\right\} \times \varphi_e(\mathbf{r}) + \frac{1}{4}\int V_x^{\text{val}}(\mathbf{r},\mathbf{r}')\varphi_e(\mathbf{r}')d\mathbf{r}' = \varepsilon_e\varphi_e(\mathbf{r}). \quad (2)$$

In the above expression we have assumed, for simplicity, a closed-shell system with $N/2$ doubly occupied one-electron states (extension to spin-polarized systems is straightforward); $V_{\text{H}}$ and $V_{\text{ion}}$ are the Hartree and the ionic (pseudo-)potentials, respectively; $V_x^{\text{PBE}}$ and $V_c^{\text{PBE}}$ are the PBE exchange and correlation potentials. We note that $V_{\text{H}}$, $V_x^{\text{PBE}}$, and $V_c^{\text{PBE}}$ are fixed operators as they only depend on the (fixed) valence charge density $\rho^{\text{val}}(\mathbf{r})=\Sigma_j^{\text{occ}}\varphi_j^*(\mathbf{r})\varphi_j(\mathbf{r})$. Finally, the nonlocal exact exchange potential $V_x^{\text{val}}(\mathbf{r},\mathbf{r}')$ is given by

$$V_x^{\text{val}}(\mathbf{r},\mathbf{r}') = -2\sum_j^{\text{occ}} \frac{\tilde{\varphi}_j^*(\mathbf{r}')\tilde{\varphi}_j(\mathbf{r})}{|\mathbf{r}-\mathbf{r}'|}, \quad (3)$$

where the sum runs over all the occupied states. This potential describes the exchange interaction between the empty state and each of the valence MLWFs $\{\tilde{\varphi}_j\}$.

The action of $V_x^{\text{val}}(\mathbf{r},\mathbf{r}')$ on the empty state $\varphi_e$ in Eq. (3) is given by

$$D_x^e(\mathbf{r}) = -2\sum_j^{\text{occ}} \int d\mathbf{r}' \frac{\tilde{\varphi}_j^*(\mathbf{r}')\varphi_e(\mathbf{r}')}{|\mathbf{r}-\mathbf{r}'|} \times \tilde{\varphi}_j(\mathbf{r}) = -2\sum_j^{\text{occ}} v_{ej}(\mathbf{r})\tilde{\varphi}_j(\mathbf{r}). \quad (4)$$

Here $v_{ej}$ is the Coulomb potential originating from the "exchange charge" $\rho_{ej}=\tilde{\varphi}_j^*(\mathbf{r}')\varphi_e(\mathbf{r}')$, and satisfies the Poisson equation

$$\nabla^2 v_{ej} = -4\pi\rho_{ej}. \quad (5)$$

It is important to note that, while the empty eigenstate of Eq. (2) is Bloch type and delocalized in real space, the exchange pair density $\rho_{ej}$ is confined by the valence MLWFs that are well localized in real space. As a result, the Poisson equation, Eq. (5), and the action of the exchange operator, Eq. (4), need only be solved in the region where $\tilde{\varphi}_j \neq 0$.

We have implemented the above computational procedure for calculating the PBE0 band gap in the CP code of the QUANTUM-ESPRESSO package.[19] The procedure works as a post processing feature following a PBE0 ground-state calculation by the MLWF-based WSC method. In this work, we use it to calculate the electronic structure, particularly the band gap, of GaN, InN, and $In_{1-x}Ga_xN$ in the zinc-blende phase. These systems are computationally challenging because InN and In-rich $In_{1-x}Ga_xN$ are incorrectly predicted to be metallic by standard GGA calculations.

TABLE I. Pseudopotential generation parameters. Here "ref." refers to the reference state occupation, $r_c$ refers to the cutoff radius, $q_c$ is the cutoff wave vector, and $N_B$ is the number of Bessel functions used for each channel (see Ref. 20).

| Atom | Parameter | *s* | *p* | *d* |
|---|---|---|---|---|
| N | ref. | 2.0 | 3.0 | |
| | $r_c$ | 1.30 | 1.30 | |
| | $q_c$ | 7.50 | 7.50 | |
| | $N_B$ | 10 | 10 | |
| Ga | ref. | 2.0 | 1.0 | 10.0 |
| | $r_c$ | 1.80 | 2.20 | 1.80 |
| | $q_c$ | 8.00 | 8.00 | 8.36 |
| | $N_B$ | 6 | 8 | 10 |
| In | ref. | 2.0 | 1.0 | 10.0 |
| | $r_c$ | 1.90 | 2.30 | 1.80 |
| | $q_c$ | 8.00 | 8.00 | 8.00 |
| | $N_B$ | 8 | 8 | 8 |

The calculations were performed using a 64-atom cubic supercell to model both $In_{1-x}Ga_xN$ and its parent compounds, GaN and InN. For each Ga concentration $x$ in the ternary $In_{1-x}Ga_xN$ compound, only a few selected atomic configurations were considered, with no specific treatment of disorder effects, as, e.g., in Refs. 4 and 8; within our limited sampling, a very weak dependence of the calculated band gap on the specific cation arrangement was observed. For direct comparison with experiments and other theoretical results, the experimental lattice constants of GaN ($a$=4.50 Å) and InN ($a$=4.98 Å) were used, while the lattice parameter of the alloy was determined by linear interpolation.

Table I shows the reference states and cutoff radii used to construct the pseudopotentials used in this study. All pseudopotentials were generated using the OPIUM code.[21] Unlike with traditional density functional theory, Hartree-Fock pseudopotentials require extra care in their construction. This arises from the nonlocal form of the Hartree-Fock exchange potential.[22–25] The presence of the nonlocal exchange potential in Hartree-Fock or Hartree-Fock/DFT hybrids will often yield pseudopotentials with an unphysical, long-range tail. A correction procedure is necessary to remove this tail and restore the correct long-range behavior of the pseudopotential while maintaining the eigenvalue spectrum and logarithmic derivatives. Recent work[22,26,27] has shown that this approach yields highly accurate Hartree-Fock pseudopotentials.

The pseudopotentials were norm-conserving/Rappe–Rabe–Kaxiras–Joannopoulos type[20] and were generated from self-consistent PBE0 all-electron reference states using the approach of Ref. 27. The Ga and In pseudopotentials were obtained from scalar-relativistic solutions while the N pseudopotential was nonrelativistic. The local potential was the *s* channel for all cases. The semicore *d* electrons were treated as valence electrons in In and Ga (this corresponds to 576 valence electrons, i.e., 288 occupied states in the 64-atom supercell). The plane-wave energy cutoff was 70 Ry

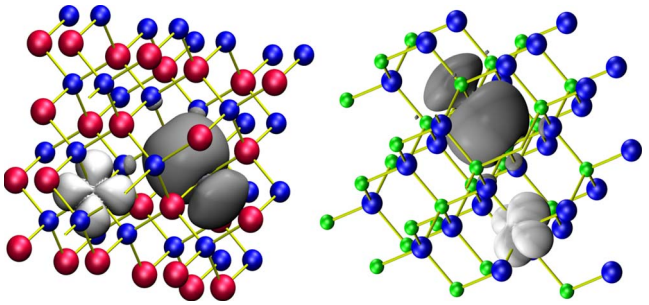

FIG. 1. (Color online) Isosurfaces of typical *d*-type and $sp^3$-type Wannier orbitals in the InN (on the left) and GaN (on the right) 64-atom supercell. The Ga, In and N atoms are denoted by the green, red, and blue spheres, respectively.

and the Brillouin zone was sampled at the Γ point. Atomic positions in the supercell were relaxed at the GGA-PBE level.

## III. RESULTS AND DISCUSSION

The PBE0 ground state was determined by the WSC method using MLWFs to calculate the exchange interaction among valence electrons.[15] While the MLWFs generated from the PBE ground state often give an excellent initial guess for the PBE0 calculations, for InN and In rich $Ga_xIn_{1-x}N$ alloy configurations, the PBE ground state shows an incorrect ordering of the energy bands. For this reason, instead of PBE Wannier orbitals we used a set of fictitious localized orbitals at the guess bonding centers as the trial solutions for Eq. (2). This procedure was essential to obtain the PBE0 ground state with correct symmetry for InN and In rich $Ga_xIn_{1-x}N$. In the empty-state calculations, for each PBE0 ground-state MLWF we first defined an orthorhombic box such that outside this box $\rho_{ej}(\mathbf{r})$ is smaller than a given cutoff value $\rho^{\text{cut}}$; we take this cutoff equal to $2 \times 10^{-4}$ bohr$^{-3}$ in the present work. Then Eq. (5) is solved by the conjugate gradient method[15] and for each pair $\rho_{ej}$ formed by the empty state and a PBE0 ground state MLWF its action Eq. (4) is applied only inside the above truncated box. Finally with this $D_x^e(\mathbf{r})$, Eq. (2) is solved via a damped second-order Car-Parrinello dynamics.[28]

Representative MLWFs for InN in its PBE0 ground state are shown in Fig. 1. Two types of valence MLWFs are present in our calculations, *d*-type Wannier orbitals centered at the In sites, and covalent $sp^3$-type orbitals centered between the cations and the anions. As one can see from the figure, the *d*-type orbitals originating from the cation semicore states are more localized than the $sp^3$-type ones. The valence MLWFs are qualitatively similar for GaN, except for a slightly more pronounced localization related to the larger band gap.

The band-structure properties of GaN and InN that result from our PBE0-MLWFs calculations are summarized in Table II. Here we report the valence-band width (VBW), the band gap $E_g$ and the average *d*-band binding energy $E_d$, and compare them to PBE calculations (performed with the same 64-atom supercell used for the PBE0 calculations) and experimental results. For further comparison, we also report the results of PBE0 calculations performed using the reciprocal-space implementation in Ref. 19; we can see that the agreement between these results and our MLWF-based calculations is very good. From Table II it appears that the GGA-PBE results significantly overestimate the energetic position of the cation *d* bands. Because of the *pd* repulsion, the overestimated *d* bands level in turn pushes the *p* band upward, resulting in an underestimated band gap. For InN, this effect leads to a wrong ordering of the $\Gamma_{1c}$ and $\Gamma_{15v}$ energy levels, and thus to the incorrect prediction of a metallic ground state. In the PBE0 calculations, the inclusion of exact exchange reduces the delocalization error. As shown by Table II, the PBE0 VBW is larger and the *d*-bands level shifts downward, in better agreement with the experiment. In turn, this leads to a considerable improvement of the band gaps of both InN and GaN with respect to experiment; in particular, the PBE0 band gap becomes 1.09 eV for InN. It is also worth noticing that calculation of the PBE0 band gap using a PBE pseudopotential yields a ~0.2 eV smaller value than that obtained with the PBE0 pseudopotential.

TABLE II. Valence-band width, band gap, and average *d*-band binding energy (eV) of GaN and InN.

| | | VBW | $E_g$ | $E_d$ |
|---|---|---|---|---|
| GaN | PBE0-MLWFs | 17.70 | 3.52 | −16.16 |
| | PBE | 16.14 | 1.60 | −13.62 |
| | PBE0, plane waves[a] | 17.72 | 3.61 | |
| | GW[b] | | 3.53 | −16.5 |
| | Experiment[c] | | 3.3 | −17.7 |
| InN | PBE0-MLWFs | 17.04 | 1.09 | −15.30 |
| | PBE results | 15.04 | −0.04 | −13.48 |
| | GW[b] | | 0.78 | −15.3 |
| | Experiment | | 0.61[b] | −16.0 [c] |

[a]Reciprocal-space method in PWSCF (Ref. 19) in two-atom cell and $4\times4\times4$ *k* points.
[b]Reference 29.
[c]Reference 30.

Besides confirming the good performance of hybrid functionals for band-gap predictions, the above results for InN and GaN provide evidence of the reliability of our procedure for calculating the PBE0 band gap. We have thus applied this procedure to the study of the ternary $In_{1-x}Ga_xN$ compound, a system for which the standard reciprocal-space approach to calculate the exact exchange would be extremely cumbersome. Instead, our order-*N* scheme is well suited to treat systems for which large supercells are needed. Using a 64-atom supercell, we then considered $In_{1-x}Ga_xN$ models with 1(31), 2(30), 3(29), 4(28), 16(16), 28(4), 29(3), 30(2), and 31(1) Ga(In) cations, which correspond to $x$=0.031, 0.063, 0.094, 0.125, 0.5, 0.875, 0.906, 0.938, and 0.969. For each value of $x$ and a given configuration of Ga(In) atoms, the atomic positions were relaxed at the PBE level. The computed PBE0 band gap of $In_{1-x}Ga_xN$ as a function of the Ga fraction $x$ is shown in Fig. 2(a), together with experimental[31] and PBE results. We can see that PBE not only significantly underestimates the band gap but incorrectly shows a metallic

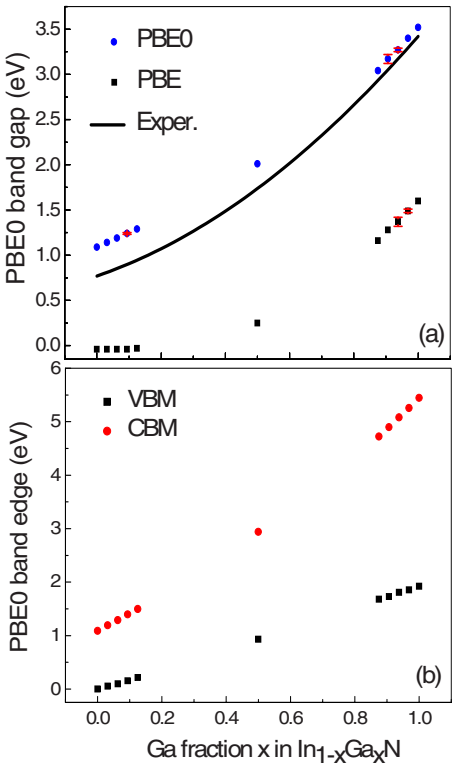


FIG. 2. (Color online) (a) PBE0, PBE, and experimental band gap of dependence Ga fraction $x$ and (b) VBM and conduction-band minimum as a function of Ga fraction $x$ in $In_{1-x}Ga_xN$.

ground state for $x<0.5$. By contrast, a direct band gap at the $\Gamma$ point is found for all values of $x$ at the PBE0 level. Moreover, PBE0 predicts a large band-gap bowing effect, in qualitative agreement with the experiment.[31] The band gap can be fitted to the quadratic form

$$E_g^{\text{alloy}} = xE_g^{\text{GaN}} + (1-x)E_g^{\text{InN}} - x(1-x)b \tag{6}$$

from which a bowing coefficient $b^{\text{PBE0}}=1.63$ eV can be extracted, similar to the value, 1.67 eV, found in previous screened-exchange density functional ($sx$-LDA) calculations.[4] However, this is somewhat larger than the experimental value $b^{\text{expt}}=1.43$ eV,[31] likely because of the overestimated PBE0 band gap for the In-rich compounds. To gain more insight into the origin of the large band-gap bowing, we have examined how the valence-band maximum (VBM) and conduction-band minimum (CBM) depend separately on $x$, see Fig. 2(b). In this analysis, the average electrostatic potential was taken as the reference for the band alignment. It can be seen that the VBM increases almost linearly with $x$, whereas the CBM shows a stronger nonlinear increase which is responsible for the large bowing coefficient of the alloy.

The electronic states in proximity of the VBM are important for the pholuminescence properties of $In_{1-x}Ga_xN$. These states have the character of $p$ orbitals localized at the N sites.

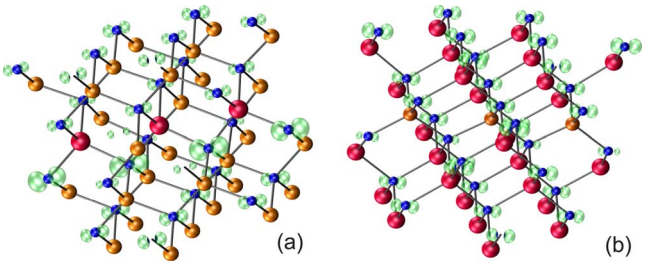


FIG. 3. (Color online) Isosurfaces of PBE0 eigenstate (a) $In_3Ga_{29}N$, where three In atoms forms a zigzag chain structure; (b) $Ga_3In_{29}N$, where three Ga atoms forms a zigzag chain N atoms are denoted by red, orange, and blue spheres, respectively.

Previous theoretical studies of $In_{1-x}Ga_xN$ found that in Ga-rich alloys the amplitude of these states is enhanced at N sites close to In impurities,[4,8] suggesting a localization of photoexcited holes at such sites. This interesting result is confirmed by our PBE0 hybrid calculations. The enhancement, or hole localization, is particularly evident when the In impurities are clustered to form a zigzag In-N-In-N-In chain, as shown in Fig. 3(a). This localization has been suggested to be the reason of the high efficiency of $In_{1-x}Ga_xN$-based emitting devices.[4,7] Interestingly, we found that there is an opposite effect for the case of Ga impurities in In rich alloys. Here, a reduction in the $p$ states at the N sites along the Ga-N-Ga-N-Ga-N chain is observed, see Fig. 3(b).

## IV. SUMMARY

In conclusion, we have described an efficient procedure to calculate the band gap of extended insulating systems using hybrid functionals. This procedure is based on the recently developed WSC order-$N$ method, in which the Hartree-Fock exchange is calculated using MLWFs, and can therefore be used to study the band gap and other electronic properties of systems with large unit cells. We have demonstrated the effectiveness of our approach by a study of the band gap of a ternary compound, $In_{1-x}Ga_xN$, that we have modeled using a 64-atom supercell. Hybrid functional results for this important material are here reported for the first time, without the approximation of screened exchange, and show a much better agreement with experiment than conventional DFT-GGA or LDA calculations. Our approach can be widely used for the band-gap engineering problem in semiconductor alloys.

## ACKNOWLEDGMENTS

This work has been supported by the Department Of Energy under Grants No. DE-FG02-06ER-46344, No. DE-FG02-05ER46201, and No. AFOSR-MURI F49620-03-1-0330. A. M. R. was supported by the (U.S.) Department of Energy under Grant No. DE-FG02-07ER46431. X.W. would like to thank Jennifer Chan and Alessandro Stroppa for useful discussions.

[1] P. Piquini, P. A. Graf, and A. Zunger, Phys. Rev. Lett. **100**, 186403 (2008); S. V. Dudiy and A. Zunger, *ibid.* **97**, 046401 (2006).
[2] A. Grüneis, K. Hummer, M. Marsman, and G. Kresse, Phys. Rev. B **78**, 165103 (2008).
[3] M. N. Huda, Y. Yan, S.-H. Wei, and M. M. Al-Jassim, Phys. Rev. B **78**, 195204 (2008).
[4] B. Lee and L.-W. Wang, J. Appl. Phys. **100**, 093717 (2006).
[5] J. W. Bennett, I. Grinberg, and A. M. Rappe, J. Am. Chem. Soc. **130**, 17409 (2008).
[6] A. Stroppa and G. Kresse, Phys. Rev. B **79**, 201201(R) (2009).
[7] S. F. Chichibu, A. Uedono, T. Onuma, B. A. Haskell, A. Chakraborty, T. Koyama, P. T. Fini, S. Keller, S. P. Denbaars, J. S. Speck, U. K. Mishra, S. Nakamura, S. Yamaguchi, S. Kamiyama, H. Amano, I. Akasaki, J. Han, and T. Sota, Philos. Mag. **87**, 2019 (2007).
[8] L. Bellaiche, T. Mattila, L.-W. Wang, S.-H. Wei, and A. Zunger, Appl. Phys. Lett. **74**, 1842 (1999).
[9] R. G. Parr and W. Yang, *Density Functional Theory of Atoms and Molecules* (Oxford University Press, New York, 1989).
[10] A. J. Cohen, P. Mori-Sanchez, and W. Yang, Science **321**, 792 (2008).
[11] A. J. Cohen, P. Mori-Sanchez, and W. Yang, Phys. Rev. B **77**, 115123 (2008).
[12] B. G. Janesko, T. M. Henderson, and G. E. Scuseria, Phys. Chem. Chem. Phys. **11**, 443 (2009).
[13] A. D. Becke, J. Chem. Phys. **98**, 1372 (1993).
[14] M. Marsman, J. Paier, A. Stroppa, and G. Kresse, J. Phys.: Condens. Matter **20**, 064201 (2008).
[15] X. Wu, A. Selloni, and R. Car, Phys. Rev. B **79**, 085102 (2009).
[16] N. Marzari and D. Vanderbilt, Phys. Rev. B **56**, 12847 (1997).
[17] J. P. Perdew, M. Ernzerhof, and K. Burke, J. Chem. Phys. **105**, 9982 (1996).
[18] J. P. Perdew, K. Burke, and M. Ernzerhof, Phys. Rev. Lett. **77**, 3865 (1996).
[19] See, http://www.quantum-espresso.org
[20] A. M. Rappe, K. M. Rabe, E. Kaxiras, and J. D. Joannopoulos, Phys. Rev. B **41**, 1227 (1990).
[21] OPIUM pseudopotential package http://opium.sourceforge.net
[22] J. R. Trail and R. J. Needs, J. Chem. Phys. **122**, 014112 (2005).
[23] D. M. Bylander and L. Kleinman, Phys. Rev. Lett. **74**, 3660 (1995); Phys. Rev. B **52**, 14566 (1995); **54**, 7891 (1996); **55**, 9432 (1997).
[24] M. Städele, J. A. Majewski, P. Vogl, and A. Görling, Phys. Rev. Lett. **79**, 2089 (1997).
[25] E. Engel, A. Höck, R. N. Schmid, R. M. Dreizler, and N. Chetty, Phys. Rev. B **64**, 125111 (2001).
[26] J. R. Trail and R. J. Needs, J. Chem. Phys. **122**, 174109 (2005).
[27] W. A. Al-Saidi, E. J. Walter, and A. M. Rappe, Phys. Rev. B **77**, 075112 (2008).
[28] R. Car, in *Conceptual Foundations of Materials: A Standard Model for Ground- and Excited-State Properties*, Contemporary Concepts of Condensed Matter Science, edited by S. G. Louie and M. L. Cohen (Elsevier, Amsterdam, 2006), Chap. 3, p. 64.
[29] F. Fuchs, J. Furthmüller, F. Bechstedt, M. Shishkin, and G. Kresse, Phys. Rev. B **76**, 115109 (2007).
[30] L. F. J. Piper, T. D. Veal, P. H. Jefferson, C. F. McConville, F. Fuchs, J. Furthmüller, F. Bechstedt, H. Lu, and W. J. Schaff, Phys. Rev. B **72**, 245319 (2005).
[31] J. Wu, W. Walukiewicz, K. M. Yu, J. W. Ager III, E. E. Haller, H. Lu, and W. J. Schaff, Appl. Phys. Lett. **80**, 4741 (2002).